Computational Research on Modular Undulating Fin for Biorobotic Underwater Propulsor

Yong-hua Zhang[1], Lai-bing Jia[1], Shi-wu Zhang[1], Jie Yang[1], K. H. Low[2]

1. *Dept of Precision Machinery and Precision Instrumentation, University of Science and Technology of China,*
Hefei 230026, P. R. China
2. *School of Mechanical and Aerospace Engineering, Nanyang Technological University, 639798, Singapore*

Abstract

Biomimetic design employs the principles of nature to solve engineering problems. Such designs which are hoped to be quick, efficient, robust, and versatile, have taken advantage of optimization via natural selection. In the present research, an environment-friendly propulsion system mimicking undulating fins of stingray was built. A non-conventional method was considered to model the flexibility of the fins of stingray. A two-degree-of-freedom mechanism comprised of several linkages was designed and constructed to mimic the actual flexible fin. The driving linkages were used to form a mechanical fin consisting of several fin segments, which are able to produce undulations, similar to those produced by the actual fins. Owing to the modularity of the design of the mechanical fin, various undulating patterns can be realized. Some qualitative observations, obtained by experiments, predicted that the thrusts produced by the mechanical fin are different among various undulating patterns. To fully understand this experimental phenomenon is very important for better performance and energy saving for our biorobotic underwater propulsion system. Here, four basic undulating patterns of the mechanical fin were performed using two-dimensional unsteady computational fluid dynamics (CFD) method. An unstructured, grid-based, unsteady Navier-Stokes solver with automatic adaptive re-meshing was used to compute the unsteady flow around the fin through twenty complete cycles. The pressure distribution on fin surface was computed and integrated to provide fin forces which were decomposed into lift and thrust. The pressure force and friction force were also computed throughout the swimming cycle. Finally, vortex contour maps of these four basic fin undulating patterns were displayed and compared.

Keywords: biomimetic, modular undulating fin, biorobotic, AUV, CFD, propulsion efficiency

1 Introduction

In the field of underwater robotics research, undulating-finned robot offers exceptional advantage over propeller in preserving an undisturbed condition of its surroundings for data acquisition. Autonomous underwater vehicle (AUV) is an interesting area of application that could also greatly benefit from biomimetic mechanical systems, as there is an increasing demand for improved efficiency to allow longer missions to be undertaken. Military and defence are the most important areas where biomimetics finds its significant role in ensuring safe; the undulating-finned robot might be undetected when swims with a school of fish and therefore may act as a spy.

Nowadays, many new concepts of biologically inspired underwater propulsion system have been developed[1–6], including several undulating-finned underwater robots[7–16]. But little attention has been paid to the detailed fluid mechanisms of the motions of these unsteady mechanical fins. In our research, we developed an underwater biorobotic propulsor mimicking undulating fins of stingray[17,18]. Owing to the modularity of the design of the mechanical fin, we were able to realize various undulating patterns. Some qualitative observations, obtained by experiments, predicted that the thrusts produced by the

Corresponding author: Yong-hua Zhang
**E-mail**: yhzhang@ustc.edu

mechanical fins are different among various fin undulating patterns. To reveal the regularity of this experimental finding is very important for better swimming performance, efficiency improvement and energy saving for our biorobotic underwater propulsion system.

Some initial work on two typical undulating patterns of the mechanical fin have already been reported[19]. In this study, we seek to complement those studies by adding more cases and efficiency calculation using two-dimensional unsteady Computational Fluid Dynamics (CFD) method. CFD simulations solve the Navier-Stokes equations, which account for all fluid mechanical effects. By using the CFD method, a lot of intricate questions could be well answered. However, the application of CFD to the case of an undulating fin can be tedious due to the large computational resources required to simulate the moving boundary of the fin. Liu and Kawachi[20,21] used the CFD method to simulate 2D and 3D hydrodynamics of Tadpole locomotion. G. Dong and Lu[22] presented several important computational results of the influence of C/U on vortex distribution. Other researchers published results of 3D unsteady computations of pectoral fin[23-25]. So far as we know, it is the first attempt to study the influence of fin undulating patterns on swimming performance using CFD method.

2 Background

Stingray and knifefish are two typical fishes which effectively propel themselves through water based on the undulating motion of their fins. Stingray possesses a pair of large pectoral fins that are greatly expanded and fused to the head. The knifefish swims with a long-based ventral fin (Fig. 1). These fins consist of fin-rays and a flexible membrane connecting them together. A set of muscle for each fin-ray provides the latter with two-degree-of-freedom movement capability. It has been suggested that certain fish can actively bend the rays of fins[26].

Thrust is produced by large undulations along fins which span from the anterior to the posterior of the fish. The amplitude envelope of the undulations is changeful, which remains a question: what kind of amplitude envelope of undulations is the best for undulating-finned biorobotic underwater propulsion system.
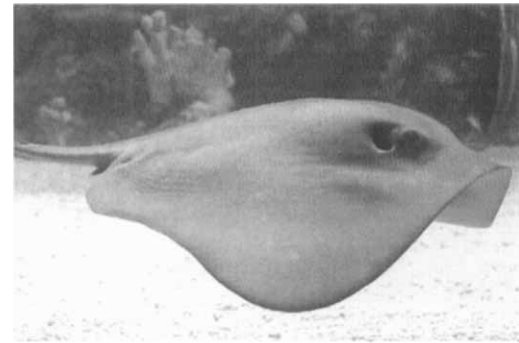
(a) Stingray
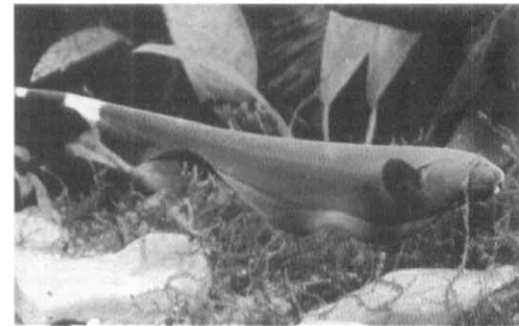
(b) Knifefish

Fig. 1 Two typical undulating fin based motion organisms.

3 Undulating-finned biorobots

3.1 Mechanical design

In order to investigate what kind of amplitude envelope provides the maximum efficiency for undulating fin propulsion, a modular undulating fin (Fig. 2) was designed and constructed. The fin can accommodate 10cm peak-to-peak amplitude, various wave speeds, amplitude envelopes, and wavelengths[17]. In line with Lighthill's conclusion[27], those variables can be summarized as

$$y(x,t) = A(x) \times \sin[2\pi(\frac{x}{\lambda} - \frac{t}{T})] , \qquad (1)$$
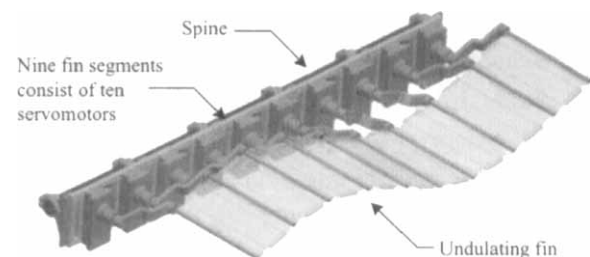

Fig. 2 A modular undulating fin consisting of ten equally spaced servomotors attached to a lightweight structure on both sides. Ten cranks representing ten fin rays, and nine fin segments[17].

where $y(x,t)$ defines the position of any fin ray along the x-axis at any time t, $A(x)$ represents any function that dictates the amplitude envelope of the fin, λ accounts for the undulating wave speed, and T accounts for the undulating period (refer to [17] for more details).

3.2 Four typical undulating patterns of the mechanical fin

Some qualitative observations predicted that the thrusts produced by the mechanical fins are different among various fin undulating amplitude envelopes. To reveal the regularity of this experimental finding, four typical undulating patterns of the mechanical fins are selected and compared using the CFD method with the same amplitude envelope area as well as other kinematics parameters such as frequency, wavelength and wave propulsion velocity (Fig. 3). The first three mechanical fin patterns (Fig. 3a, Fig. 3b, Fig. 3c) are similar to nature organisms (the black ghost, cuttlefish, rays) respectively, while the fourth pattern is selected for comparison.

The black ghost propels itself by oscillating the ribbon fin rays slightly out of phase, thereby producing a traveling wave along the fin, while keeping its thin, flat

body mostly rigid. The wave travels in the direction opposite to that of the body's motion with its amplitude envelope gradually increaseing from the anterior part to the posterior part, as shown in Fig. 3a[14]. Cuttlefish is also observed using its fin for low speed swimming. In smaller and narrow-finned cuttlefish, the amplitude envelope is fairly constant along the fins, as shown in Fig. 3b[18]. The amplitude envelope of the rays increases from the anterior part to the fin apex and decreases toward the posterior part, as shown in Fig. 3c. Such amplitude envelope can be explained from its triangular shaped pectoral fins; they are narrower toward the anterior and posterior parts of the fish.

The function that dictates the amplitude envelope of the fin shown in Fig. 3 is expressed in Eq. (2), where h is the peak-to-peak amplitude, L is the fin length.
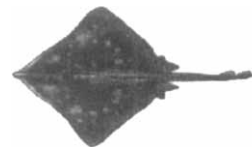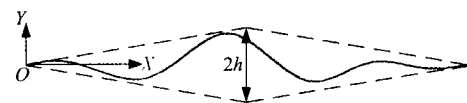
$$A(x) = \begin{cases} \dfrac{2x}{L}h & \text{(a)} \\[2mm] \dfrac{4h}{L}\left|x - \dfrac{L}{2}\right| & \text{(b)} \\[2mm] 2h - 2h\left|1 - \dfrac{2x}{L}\right| & \text{(c)} \\[2mm] h & \text{(d)} \end{cases} \tag{2}$$
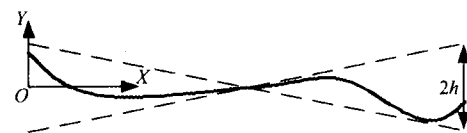

(a) The amplitude envelope gradually increases from the anterior part to the posterior.
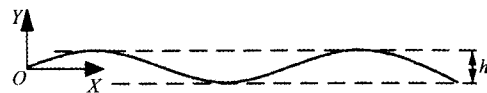
(b) The amplitude envelope is fairly constant along the fins.

(c) The amplitude envelope increases from the anterior part to the mid part and decreases toward the posterior.

(d) The amplitude envelope decreases from the anterior part to the mid part and increases toward the posterior.

Fig. 3 Four typical amplitude envelopes of modular undulating fins (photos are taken from [28]).

4 Materials and methods

4.1 Mathematic model

The fluid is supposed to be incompressible and unsteady, so the control equations are the continuity equation and time related Navier-Stokes equation and are given as

$$\frac{\partial W}{\partial t} + \frac{\partial F_I}{\partial x} + \frac{\partial G_I}{\partial y} = \frac{\partial F_V}{\partial x} + \frac{\partial G_V}{\partial y},$$

$$W = \begin{bmatrix} \rho \\ \rho u \\ \rho v \end{bmatrix} \quad F_V = \begin{bmatrix} 0 \\ \tau_{xx} \\ \tau_{xy} \end{bmatrix} \quad G_V = \begin{bmatrix} 0 \\ \tau_{yx} \\ \tau_{yy} \end{bmatrix}, \quad (3)$$

$$F_I = \begin{bmatrix} \rho u \\ \rho u^2 + p \\ \rho u v \end{bmatrix} \quad G_I = \begin{bmatrix} \rho v \\ \rho u v \\ \rho v^2 + p \end{bmatrix},$$

where x and y are the axes of the orthogonal coordinate system, while u and v are the fluid velocity vectors in x, y direction respectively, p is the pressure, and ρ is the fluid density. Turbulence quantities were not considered in the governing equations because the laminar flow was assumed for this computation. All the fluid variables were made dimensionless with respect to the uniform inflow U, the fin length L, and the fluid density ρ respectively. The dimensionless parameter of the Reynolds number (Re) is defined as

$$Re = UL / v, \quad (4)$$

where v is the kinematic viscosity, with a value of 1.533×10^{-6} $m^2 \cdot s^{-1}$. Given a body length of 0.05 m in our model and a reasonable and realistic forward swimming speed of 0.06 $m \cdot s^{-1}$, we can calculate a Re of about 2000. The governing equations were discretized using the finite volume method (FVM) with an implicit segregated solver approach. The Navier-Stokes momentum equations were discretized with a second order upwind scheme, while pressure was interpolated using a second order accurate scheme. An implicit first order scheme was used for temporal discretization, with a time step size of 0.001 second. Simulations were carried out for 6000 time steps to simulate swimming for twenty tail-beat periods. Pressure velocity coupling of the continuity equation was achieved using the SIMPLE algorithm that is valid for the small time steps used in the simulation.

4.2 Convergence

For each time step residuals of the continuity equation, x-velocity, and y-velocity all typically converged in less than 50 iterations to a scaled residual of 0.001. Several time steps were examined more closely and the results showed solution convergence was achieved. Grid convergence was tested using the Richardson extrapolation method described by Celik and Karatekin[29]. Several parameters describing the vortices in the wake were tested and the results showed that grid convergence for the fine mesh was achieved within 0.6% of the extrapolated exact values.

4.3 Unstructured mesh generation and adaptive re-meshing

If the bodies move through the flow field, the positions of relevant flow features will change. Therefore, in most of the computational domain, a new mesh distribution is required. One approach to solve these problems is to add a moving grid system. Accordingly, we made the grids fit the deforming boundaries at each physical time step, and also made sure that there was sufficient grid density to resolve the viscous and unsteady flows both around the body surface and in the wake. As the elements (or edges) move, their geometric parameters (shape–function derivatives, etc.) need to be recomputed at each time step. If the whole mesh is assumed to be in motion, then these geometric parameters need to be recomputed globally. In order to reduce the number of global remeshings and computation load, only a small number of elements surrounding the bodies are actually moved. The remainder of the field is then treated in the usual Eulerian frame of reference, avoiding recomputing geometric parameters. Details of the algorithm can be found in the work by Ramamurtil et al.[23].

The computational mesh consists of 16 844 nodes and 32 986 triangular elements, which is sufficient for resolving the inviscid flow through this configuration. The boundary condition for the inlet was velocity inlet. The downstream boundary was modeled as a constant pressure outlet while the sides were modeled as no-slip walls. And both of the fin surfaces were simulated as a smooth no-slip wall (see Eq. (5)).

$$u_i = u_{i\infty} \quad \frac{\partial u_i}{\partial n} = 0 \quad p = p_\infty \quad \frac{\partial p}{\partial n} = 0 \quad (5)$$

The undulating fin parameters for computation are listed in Table 1.

Table 1 Undulating fin parameters for computation

Parameter	Description	Value
λ	Propulsion wavelength	0.025 m
T	Propulsion period	0.25 s
t	Computational time	6 s
x	Horizontal position	$0 < x < 0.05$ m
L	Fin length	0.05 m
h	Fin amplitude	0.004 m
$A(x)$	Function of amplitude envelope	Refer to Eq. (2)

5 Results and discussion

5.1 Pressure distribution

Pressure contours (Pa) of the flow field of the four fin undulating patterns at U=0.06 m·s^{-1} (Re = 1957), t = 6 s are compared in Fig. 4. The t = 6 s was selected because the pressure at this moment approximates the average value. The negative and positive pressure re-

gions are greatly developed through the undulating motion of mechanical fin. Thus this pressure differences result in generation of propulsion force.

5.2 Pressure force vs. friction force

The period-averaged pressure force and friction force were calculated as listed in Table 2. These forces are the results of the interaction between fin and fluid, where pressure force is caused by pressure difference and friction force is caused by water viscidity.

**Table 2 Period-averaged thrust and drag computation for the four fin undulating patterns**

Fin undulating pattern	Pressure force (N)	Friction force (N)	Net force (N)	Efficiency (%)
Fig. 3a	−0.01576	0.01143	−0.00433	57.9
Fig. 3b	−0.00369	0.00921	0.00552	28.6
Fig. 3c	−0.00236	0.00948	0.00712	19.9
Fig. 3d	−0.00911	0.00877	−0.00034	50.9
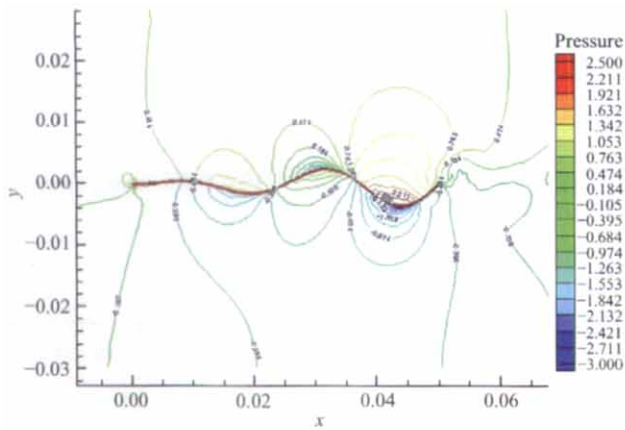
(a) The amplitude envelope gradually increases from the anterior part to the posterior.
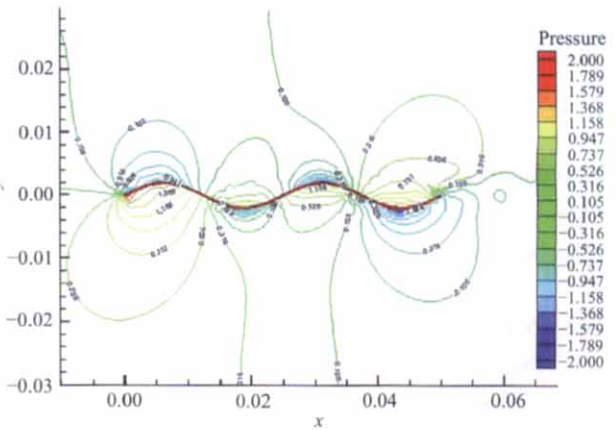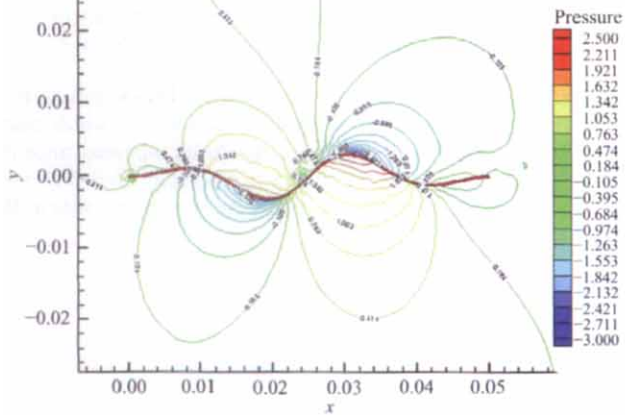
(b) The amplitude envelope is fairly constant along the fins

(c) The amplitude envelope increases from the anterior part to the mid part and decreases toward the posterior.
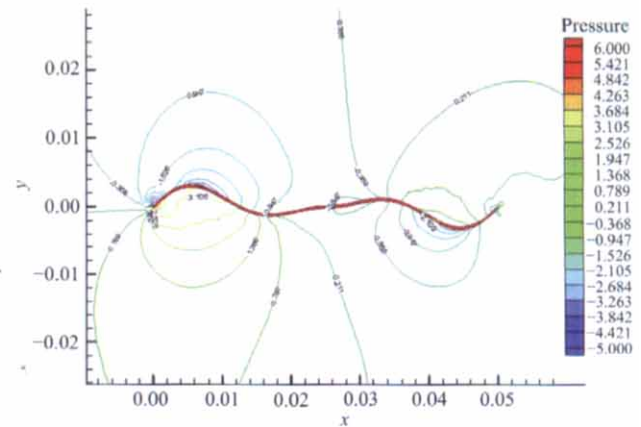
(d) The amplitude envelope decreases from the anterior part to the mid part and increases toward the posterior.

Fig. 4 Pressure contours (Pa) of the flow field of the four fin undulating patterns at U=0.06 m·s^{-1}, t = 6 s (Re = 1957).

The pressure force is divided into thrust (expressed as negative value) and drag (expressed as positive value). When thrust is larger than drag, the value of pressure force will be negative as shown in Table 2. Here, we define the efficiency as

$$\text{Efficiency} = \frac{\text{Pressure force}}{\text{Pressure force}+\text{Friction force}} \times 100\% . \quad (6)$$

From Table 2, we can see that the undulating fin motion with the amplitude envelope gradually increasing from the anterior part to the posterior (Fig. 3a) produces the higher thrust and efficiency than the other three patterns with the same other kinematics parameters. The undulating fin motion with the constant amplitude envelope (Fig. 3b) produces larger thrust and efficiency than the pattern with the amplitude envelope increasing from the anterior part to the mid part and decreasing toward the posterior (Fig. 3c). These simulation results accord with the biology conclusion that the black ghost swims much faster and effectively than cuttlefish/rays. And rays are often regarded as awkward swimmers. However, there is an interesting discovery that the amplitude envelope decreasing from the anterior part to the mid part and increasing toward the posterior (Fig. 3d) has the second highest swimming efficiency but without any biology reference.

5.3 Wake characteristics

The wake of four fin undulating patterns at $t = 6$ s was dominated by a reverse von Karman vortex street with a downstream directed jet behind the model. The alternating shedding vortices in the wake are evident in the contour plot of vorticity (Fig. 5). The vorticity vector (ω) is a measure of the rotation of the flow field and is equal to the curl of the velocity vector, which for two-dimensional flow reduces to

$$\omega_z = \frac{\partial v}{\partial x} - \frac{\partial u}{\partial y} , \quad (7)$$

ω has the unit of s^{-1}. Positive vorticity represents rotation in the counter clockwise direction, while negative vorticity represents rotation in the clockwise direction.

Vorticity develops along the entire length of the fin and is shed into the wake at the position where the posterior part is into the wake, as seen in Fig. 5a, Fig. 5b and Fig. 5d. This vorticity has opposite rotation on each side

of the fin due to the boundary layer; thus vortices in the wake can easily be traced back to the side of the fin where they originated from. The vorticity bound originally to the right side of the body is shed to the left side of the wake, and vice versa. However, the third fin undulating pattern that the amplitude envelope increases from the anterior part to the mid and decreases toward the posterior is somewhat different, as seen in Fig. 5c. In this case, the vorticity develops along the anterior part of the fin and is shed into the wake at the position where the middle part is into the wake. This early separation of vortex may lead to less thrust generation and increase in drag.

(a) The amplitude envelope gradually increases from the anterior part to the posterior

(b) The amplitude envelope is fairly constant along the fins

(c) The amplitude envelope increases from the anterior part to the mid part and decreases toward the posterior

(d) The amplitude envelope decreases from the anterior part to the mid part and increases toward the posterior.

Fig. 5 Vorticity (s^{-1}) contours around the fin swimming at U = 0.06 m·s^{-1}, $t = 6$ s. Positive vorticity indicates counterclockwise rotation of the fluid, whereas negative vorticity indicates clockwise rotation. Note how vorticity is shed into the wake from only one side of the fin in each instance.

6 Conclusion and future works

In this paper, the following aspects have been discussed:

(1) An environment-friendly propulsion system mimicking undulating fins of stingray was built.

(2) Four basic undulating patterns of the mechani-

cal fin were performed using two-dimensional unsteady CFD method.

(3) The pressure distributions on fin surfaces were computed and integrated to provide fin forces which were decomposed into lift and thrust.

(4) The period-averaged pressure force and friction force were calculated.

(5) The swimming efficiencies of these four patterns were compared.

(6) The vortex shedding mechanisms and the wakes of these four basic fin undulating patterns were investigated using the simulation dataset.

The model simulation was not without problems, accurate fin shapes were not accounted for and the flow was two-dimensional. To better evaluate the model while swimming mechanisms have been investigated, the next step should be more other fin kinematics cases for comparison of different mechanisms. These could be accomplished by varying the wave speed, the wavelength, amplitude envelope functions, or several other parameters. Adding turbulence and creating a three-dimensional simulation would provide the most accurate and realistic numerical simulation for this undulating-finned biorobotic underwater propulsor.

Acknowledgement

References

[1]   Bandyopadhyay P R. Maneuvering hydrodynamics of fish and small underwater vehicles. *Integrative and Comparative Biology*, 2002, **42**, 102–117.

[2]   Ono N, Kusaka M, Taya M, Wang C. Design of fish fin actuators using shape memory alloy composites. Smart structures and materials: Industrial and commercial applications of smart structures technologies, Eric H. Anderson (ed). *Proceedings of SPIE*, 2004, **5388**, 305–312.

[3]   Guo S, Okuda Y, Asaka K. A novel type of underwater micro biped robot with multi DOF. *Proceedings of the 2004 IEEE International Conference on Robotics and Automation*, 2004, 4881–4886.

[4]   Liu J, Hu H. Mimicry of sharp turning behaviours in a robotic

fish. *Proceedings of the 2005 IEEE International Conference on Robotics and Automation*, Barcelona, Spain, 2005, 3329–3334.

[5]   Liu J, Dukes Ian, Hu H. Novel mechatronics design for a robotic fish. 2005 *IEEE/RSJ International Conference on Intelligent Robots and Systems*, Edmonton, AB, Canada, 2005, 2077–2082.

[6]   Kodati P, Deng X. Towards the body shape design of a hydrodynamically stable robotic boxfish. 2006 *IEEE/RSJ International Conference on Intelligent Robots and Systems*, Beijing, China, 2006.

[7]   Michael F, David M L, Bruce C D. An experimental undulating-fin device using the parallel bellows actuator. *Proceedings of the 2001 IEEE International Conference on Robotics and Automation*, Seoul, Korea, 2001.

[8]   Brian P T, Kerr J L, Sridhar K. Biomimetic compliant system for smart actuator-driven aquatic propulsion: Preliminary results. *Proceedings of IMECE'03 2003 ASME International Mechanical Engineering Congress*, Washington DC, USA, 2003.

[9]   Andres P, Mart A, Maarja K. A biologically inspired ray-like underwater robot with electroactive polymer pectoral fins. *IEEE Mechatronics and Robotics (MechRob'04)*, Aachen, Germany, 2004, 241–245.

[10]   Malcolm A M, Ebraheem F, Joel W B. Designing future underwater vehicles: Principles and mechanisms of the weakly electric fish. *IEEE Journal of Oceanic Engineering*, 2004, **29**, 651–659.

[11]   Epstein M, Colgate J E, MacIver M A. A biologically inspired robotic ribbon fin. *Proceedings of IEEE/RSJ International Conference on Intelligent Robots and Systems*, Edmonton, Alberta, Canada, 2005.

[12]   Hu T J, Li F, Wang G M, Shen L C. Morphological measurement and analysis of *Gymnarchus Niloticus*. *Journal of Bionics Engineering*, 2005, **2**, 25–31,.

[13]   Hu T J, Li F, Shen L C. A contour-detecting algorithm for undulation by the long-based dorsal fin of *Gymnarchus Niloticus*. *Journal of National University of Defense Technology*, 2005, **27**, 62–66, in Chinese .

[14]   Epstein M, Colgate J E, MacIver M A. Generating thrust with a biologically-inspired robotic ribbon fin. 2006 *IEEE/RSJ International Conference on Intelligent Robots and Systems (IROS), Special Session on Robotic Fish*, 2006, Beijing, China.

[15]   Zhang Y, He J, Yang J. Design and investigation of shape memory alloy dce on robotics and biomimetics. *Proceedings of the IEEE International Conference on Robotics and*

Biomimetics (ROBIO2006), Kunming, China, 2006.

[16] Zhang Y, He J, Yang J, Low K H. Initial research on development of a flexible pectoral fin using shape memory alloy. Proceedings of the 2006 International Conference on Intelligent Mechatronics and Automation (ICMA2006), Luoyang, China, 2006.

[17] Low K H, Willy A. Development and initial investigation of NTU robotic fish with modular flexible fins. Proceedings of the IEEE International Conference on Mechatronics & Automation (ICMA2005), Niagara Falls, Canada, 2005.

[18] Willy A, Low K H. Initial experimental investigation of undulating fin. Proc. of 2005 IEEE/RSJ Int. Conf. on Intelligent Robots and Systems (IROS 2005), Edmonton, AB, Canada, 2005.

[19] Zhang Y, Zhang S, Yang J. A CFD simulation research on undulating mode of biomimetic fish fin. Journal of System Simulation, 2006, in press.

[20] Liu H, Kawachi K. A numerical study of undulatory swimming. Journal of Computational Physics, 1999, 155, 223–247.

[21] Liu H, Kawachi K. The three-dimensional hydrodynamics of tadpole locomotion. The Journal of Experimental Biology, 1997, 200, 2807–2819.

[22] Dong G J, Lu X Y. Numerical analysis on the propulsive performance and vortex shedding of fish-like travelling wavy plate. International Journal for Numerical Methods in Fluids,

2005, 48, 1351–1373.

[23] Ramamurtil R, Sandberg W C, Lohner R, Walker J A, Westneat M W. Fluid dynamics of flapping aquatic flight in the bird wrasse: Three-dimensional unsteady computations with fin deformation. The Journal of Experimental Biology, 2002, 205, 2997–3008.

[24] Suzuki H, Kato N. A numerical study on unsteady flow around a mechanical pectoral fin. International Journal of Offshore and Polar Engineering, 2005, 15, 161–167.

[25] Zhang Y, He J, Yang J, Zhang S. A computational fluid dynamics (CFD) analysis of an undulatory mechanical fin driven by shape memory alloy. International Journal of Automation and Computing, 2006, 3, 374–381.

[26] Sfakiotakis M, Lane D M, Davies J B C. Review of fish swimming modes for aquatic locomotion. IEEE Journal of Oceanic Engineering, 1999, 24, 237–252.

[27] Lighthill M J. Large-amplitude elongated-body theory of fish locomotion. Proceedings of the Royal Society of London, A, 1971, 179, 125–138.

[28] Davies J B C, Deacon B, Lane D M, Sfakiotakis M. FLexible Appendage for Positioning and Stabilisation, Heriot-watt University, Edinburgh, Scotland, http://www.ece.eps.hw. ac. uk/ oceans/projects/flaps/describe.htm, [2006-12-11].

[29] Celik I, Karatekin O. Numerical experiments on application of Richardson extrapolation with nonuniform grids. Journal of Fluids Engineering, 1997, 119, 584–590.